Acta Cryst. (1976). A32, 216

A Cluster Model for the Transition from the Short-Range Order to the Long-Range Order State in F.c.c. Based Binary Systems and its Study by Means of Electron Diffraction

BY R. DE RIDDER, G. VAN TENDELOO AND S. AMELINCKX*

Rijksuniversitair Centrum Antwerpen, Middelheimlaan 1, *B*-2020 *Antwerpen, Belgium*

(*Received* 14 *July* 1975; *accepted* 7 *September* 1975)

The 'transition' state in binary, f.c.c. based systems is assumed to be characterized by the repetition of interpenetrating polyhedral clusters of atoms occupying lattice sites and having the macroscopic composition. Its mathematical formulation leads to relations between the short-range order (SRO) coefficients, which in turn impose conditions on the distribution in reciprocal space of the diffuse intensity as observed in electron diffraction patterns. It follows that for a given cluster type the diffuse intensity can only differ from zero along certain surfaces or curves. The effect of deviations from the ideal composition of the clusters is briefly discussed. The theory allows an explanation of available diffraction data on certain binary alloys in the initial stages of ordering *i.e.* in the 'transition' state between the SRO state and the long-range order (LRO) state.

Introduction

Following the original suggestion of Brunel, de Bergevin & Gontrand (1972), Sauvage & Parthé (1974) have developed a method to interpret the diffuse intensity distribution in electron diffraction patterns due to SRO in disordered ternary derivative structures.

The basic principle of the method consists of a generalization of one of Pauling 's rules governing the structure of ternary and quaternary ionic ordered systems (Pauling, 1960).

The crystal structure is considered to be built by the regular arrangement of identical polyhedra of ions, within which ionic disorder may exist. However, according to Pauling's electrostatic valence rule it is required that within each of the polyhedra the composition should be the same as the overall composition of the crystal. Expressing this requirement for each type of polyhedron leads to a relation between the SRO parameters, which in turn yields the geometrical loci of points in reciprocal space for which the diffuse intensity is non-vanishing. Although it is quite clear that Pauling's rule can only be applied as such to ionic crystals, we shall propose a somewhat similar guiding principle for binary alloys derived from considerations concerning the structure of LRO alloys based on the f.c.c. structure.

Quite generally the structure of any crystal can, by definition, be generated by the translation of the unit cell and its contents which, in a perfectly ordered stoichiometric alloy, has necessarily the macroscopic composition. However, in all f.c.c. based alloys which we have considered so far, one can also find smaller units,usually a simple polyhedron such as a tetrahedron having the macroscopic composition, and the LRO structure can be built by repetition of these units without necessarily maintaining the same orientation. All of the different allowed orientations of the unit in one domain of the LRO alloy can in fact be obtained by applying the symmetry operations of the point group to one such unit. All orientations which are possible in the 'transition' state of the alloy can be obtained by applying moreover all operations of the variant generating group to the previously obtained orientations. We assume that these units are also of fundamental significance to the 'transition' state, which in this context becomes a 'prefiguration' of the LRO state, in the sense that only local rearrangements are required to form microdomains of long-range order.

Even when imposing the macroscopic composition on the smallest clusters (polyhedra) compatible with the structure a certain amount of freedom or possible disorder is still left. We shall illustrate this point by means of an example.

Let us first consider the CuAu structure. We accept as a fundamental unit the tetrahedron, which can have the ideal composition Cu_2Au_2. Let us start with the tetrahedron 3, 4, 8, 7 of Fig. 1. One can obviously build the complete structure by repetition of such tetrahedra, which can of course be differently oriented *e.g.* as in 8, 7, 12, 13 which is the mirror image of 3, 4, 8, 7 whereas 5, 3, 9, 8 differs from 3, 4, 8, 7 by a 90° rotation.

The composition requirement for one cluster type is clearly not sufficient to determine unambiguously the LRO structure. This is illustrated in Fig. 2, which shows that after having built the tetrahedron 3, 4, 8, 7 one can continue with the tetrahedron 5, 3, 9, 8 either in the way shown in Fig. 2(*a*) or in the way shown in Fig. 2(*b*). The latter constitutes the first step of introducing an antiphase boundary. For each new step we have a similar choice. Quite analogous considerations apply to the other types of superstructures of the f.c.c. structure. This is the type of randomness which we assume in our model to be characteristic of the 'transition' state in a stoichiometric alloy slightly above the critical temperature for ordering, and at the early ordering stages in quenched alloys. In reality the composition requirement presumably will not be obeyed

* Also at S.C.K.-C.E.N., Mol (Belgium).

strictly. We shall consider in what way this affects our conclusions. Deviations from the composition requirement will necessarily occur in a non-stoichiometric alloy, and they will also occur in stoichiometric alloys, with greater frequency at increasing temperatures above the critical temperature for LRO. In a totally disordered alloy the distribution of clusters of a given polyhedra type is a binomial one.

Justification for the validity of our assumption for certain alloys can be deduced from the computer simulations of Gehlen & Cohen (1965) for the SRO state, from calculations based on the probability variation method of Clapp (1971) and from the results of Gragg, Bardhan & Cohen (1971). Clapp computed the frequency distribution for clusters with dimensions of f.c.c. and b.c.c. unit cells at temperatures slightly above the critical temperature (Clapp, 1971). In Table 1 we present the frequency distribution in the Cu_3Au structure for a simpler cluster type, *i.e.* for a tetrahedron of nearest neighbours in the f.c.c. lattice. The calculations were performed on the basis of a modified form of Clapp's probability variation method. As input data the SRO parameters obtained by Moss for temperatures 405 and 450 °C were used (Moss, 1964).

Table 1. *Frequency distribution of tetrahedral clusters in* Cu_3Au

	Relative frequency	
	$T=450$ °C $\left(\frac{T}{T_c}=1{\cdot}10\right)$	$T=405$ °C $\left(\frac{T}{T_c}=1{\cdot}03\right)$
Composition	$\alpha_1=-0{\cdot}195$	$\alpha_1=-0{\cdot}218$
Au_4	0·000	0·0000
Au_3Cu	0·003	0·0013
Au_2Cu_2	0·148	0·1257
$AuCu_3$	0·696	0·7446
Cu_4	0·153	0·1284

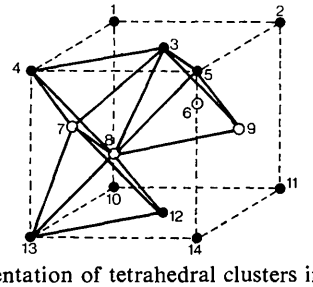

Fig. 1. Representation of tetrahedral clusters in the $L1_0$ structure all having the macroscopic composition 2:2.

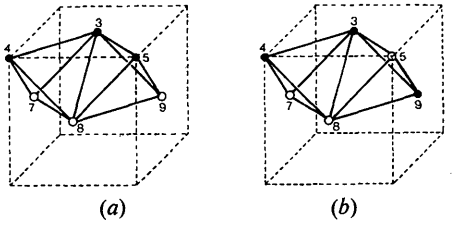

Fig. 2. Illustration of two different positions for a pair of tetrahedral clusters with the same composition but leading to different structures.

One can deduce from the results that even at the highest temperatures considered the majority of tetrahedra have the macroscopic composition. At a temperature closer to the critical temperature the frequency of tetrahedral clusters with the macroscopic composition becomes even more dominant.

On the basis of these considerations we feel that it is justified to attribute the overall aspect of the transition-state diffuse scattering to the predominant clusters of a specific type which in a stoichiometric alloy are those with the macroscopic composition. The interest of this approach lies in the fact that although the model is only approximate it is sufficiently simple to yield analytical expressions for the loci of the diffuse scattering in reciprocal space. Hence it becomes possible to interpret these patterns directly in terms of the predominant clusters of atoms.

Also it is possible, as we shall see, to take into account to some extent the effect of the occurrence of a minority of clusters which do not have the macroscopic composition.

1. The model

We shall consider the structure of an ordering system, which we will assume to be based on a f.c.c. lattice, to be built of polyhedra, all of the same type. In the f.c.c. structure it is an obvious choice to consider the structure as consisting of tetrahedra or octahedra. Furthermore we shall assume that each of these tetrahedra or octahedra will, as far as possible, have the same composition as the bulk.

For an alloy with composition AB both polyhedra are *a priori* equally acceptable since both can have the equiatomic composition. For more complicated compositions it will be necessary to assume that tetrahedra or octahedra with two different compositions may occur in a proportion which is consistent with the bulk composition. In structures with a lower symmetry, clusters of the appropriate form compatible with the symmetry of the structure and with the composition of the alloy must be assumed. We shall see examples of this in the alloys Ni–Mo and Au–V.

The form of the clusters has to be such that regular repetition may finally lead to the LRO structure. This model therefore implicitly assumes that the transition from SRO to LRO proceeds through the formation of microdomains and their subsequent growth. In this paper only the diffuse scattering associated with the initial stages of ordering, *i.e.* the transition state is considered.

2. Relations between SRO parameters

We shall show that the assumptions made in the previous paragraph lead to relations between the Warren–Cowley SRO parameters. We shall make use of a notation introduced by Flinn (1956). The occupation of the site at $\mathbf{r}_j$ is described by σ_j^{A}, which will be 1

when the site is occupied by an A atom and 0 when occupied by a B atom. In the latter case $\sigma_j^B=1$. The average values of the occupation operators σ_j^A and σ_j^B are the atom fractions m_A and m_B respectively. Deviations from the average values m_A and m_B are described by the Flinn operator $\bar{\sigma}_j$:

$$\bar{\sigma}_j=m_A-\sigma_j^A=\sigma_j^B-m_B \quad (m_A\geq m_B). \tag{1}$$

The pair probability $P_{\mathbf{R}ij}^{AB}=P_{ij}^{AB}$ for an atom A to be on the site i and an atom B to be on the site j, such that the vector $\mathbf{R}_{ij}=\mathbf{r}_i-\mathbf{r}_j$ connecting the two atoms is constant, is then given by:

$$P_{ij}^{AB}=m_Am_B-\langle\bar{\sigma}_i\bar{\sigma}_j\rangle\,.$$

The definition of the Warren–Cowley SRO parameters α_{ij} is based on the conditional probability $P_{i/j}^{AB}$ of finding a B atom on the site j assuming the site i to be already occupied by an A atom (Cowley, 1950; Warren, 1969); one has:

$$\alpha_{ij}=1-(P_{i/j}^{AB}/m_B)=1-(P_{i/j}^{AB}/m_A). \tag{2}$$

The α_{ij} are related to the average of the product of Flinn operators by the relation (see Clapp & Moss, 1966):

$$\alpha_{ij}=\langle\bar{\sigma}_i\bar{\sigma}_j\rangle/m_Am_B\,. \tag{3}$$

We shall now derive the relation between the α_{ij} that follows from our geometrical model. Let the basic polyhedron or cluster consists of S_0 lattice points ($S_0=4$ for a tetrahedron, $S_0=6$ for an octahedron, *etc.*). The numbers of A and B atoms in a cluster will be respectively S_0m_A and S_0m_B; these are necessarily integers. This condition will limit the choice of the basic unit for a given composition, and for a given type of cluster it will limit the composition. Within such a cluster there are S_1 first neighbours, S_2 second neighbours, *etc.* Numbering the points of the cluster by $1,\ldots,S_0$, one has of course:

$$\sum_{j=1}^{S_0}\sigma_j^A=m_AS_0$$

and since $\sigma_j^A=m_A-\bar{\sigma}_j$, one has:

$$\sum_{j=1}^{S_0}\bar{\sigma}_j=0\,. \tag{4}$$

In order to introduce the SRO parameters we square equation (4) and take the average over the crystal:

$$\sum_{j=1}^{S0}\langle\bar{\sigma}_j^2\rangle+2\sum_{\substack{i<j\\ i,j=1}}^{S0}\langle\bar{\sigma}_i\bar{\sigma}_0\rangle=0$$

or:

$$S_0\alpha_0+2S_1\alpha_1+2S_2\alpha_2+\ldots=0 \tag{5}$$

where for simplicity we have introduced: $\alpha_0=\alpha_{ii}=1$, α_1 corresponds to the nearest neighbours, α_2 to the second-nearest neighbours, *etc.* For the f.c.c. structure this means explicitly:

$$\alpha_1=\alpha_{000;\,\frac{1}{2}\frac{1}{2}0};\ \alpha_2=\alpha_{000;\,100};\ \alpha_3=\alpha_{000;\,1\frac{1}{2}\frac{1}{2}};\ \ldots$$

Equation (5) is of fundamental importance in this context. In the particular case of a tetrahedral cluster of nearest neighbours it becomes:

$$1+3\alpha_1=0 \tag{6}$$

and for the octahedral arrangement:

$$1+4\alpha_1+\alpha_2=0 \tag{7}$$

because there are four nearest neighbours and one second-nearest neighbour for each atom in the cluster.

Equation (5) was already derived from geometrical considerations by Sauvage & Parthé (1974).

3. SRO coefficients and diffuse intensity distribution I_D

The relationship between the SRO parameters and the diffuse intensity distribution $I_D(\mathbf{g})$ is given by (see for instance Clapp & Moss, 1966):

$$\alpha_{ij}=C\int_{V^*}I_D(\mathbf{g})\exp\left[2\pi i(\mathbf{r}_i-\mathbf{r}_j)\,.\,\mathbf{g}\right]d\mathbf{g} \tag{8}$$

where V^* represents the volume of the unit cell in reciprocal space. C is a constant for a given alloy; it can be determined from the normalization condition:

$$\alpha_0=C\int_{V^*}I_D(\mathbf{g})d\mathbf{g}=1\,. \tag{9}$$

These equations allow a derivation of the SRO parameters from the measured diffuse intensity distribution, but we shall use them conversely in order to determine qualitatively the geometry of $I_D(\mathbf{g})$ for a given model of a transition state system, which can then be compared with the observed distribution. Replacing in (5) the α_{ij} by their full expressions leads to an equation of the type:

$$\int_{V^*}I_D(\mathbf{g})F(\mathbf{g})d\mathbf{g}=0 \tag{10}$$

where:

$$\begin{aligned}F(\mathbf{g})&=\sum_{i=1}^{S_0}\sum_{j=1}^{S_0}\exp\left[2\pi i\mathbf{g}\,.\,(\mathbf{r}_i-\mathbf{r}_j)\right]\\&=\sum_{i=1}^{S_0}\exp\left[2\pi i\mathbf{g}\,.\,\mathbf{r}_i\right]\sum_{j=1}^{S_0}\exp\left[-2\pi i\mathbf{g}\,.\,\mathbf{r}_j\right].\end{aligned}$$

The indices i and j are in fact dummy indices which have to be extended over the same integers. Putting:

$$f(\mathbf{g})=\sum_{j=1}^{S_0}\exp\left[2\pi i\mathbf{g}\,.\,\mathbf{r}_j\right] \tag{11}$$

one can write:

$$F(\mathbf{g})=f(\mathbf{g})f^*(\mathbf{g})=|f(\mathbf{g})|^2\,.$$

Since $F(\mathbf{g})=|f(\mathbf{g})|^2$ is positive except perhaps for surfaces or lines in reciprocal space along which $f(\mathbf{g})=0$ and since in any case $I_D(\mathbf{g})\geq 0$ the integral (10) can only vanish if there are no non-zero contributions. This means that $I_D(\mathbf{g})$ can only differ from zero along the

surfaces or lines along which $F(\mathbf{g})$ vanishes. The shape of the diffuse intensity distribution can then qualitatively be deduced from the geometrical locus:

$$f(\mathbf{g})=0\,. \tag{12}$$

One can show that also the converse is true: if all diffuse intensity due to the transition state is concentrated along the locus $F(\mathbf{g})=0$ then all clusters corresponding to the particular form of $F(\mathbf{g})$ have the bulk composition.

If the cluster has a centre of symmetry which is not occupied by a cluster atom, one has:

$$\mathbf{r}_j=\mathbf{R}_0\pm\varrho_j(j=1,\ldots,\tfrac{1}{2}S_0;\ S_0 \text{ even})$$

where $\mathbf{R}_0$ is the position vector of the centre of symmetry. One then finds:

$$f(\mathbf{g})=2\exp\left[2\pi i\mathbf{g}\,.\,\mathbf{R}_0\right]\sum_{j=1}^{1/2S_0}\cos 2\pi\mathbf{g}\,.\,\varrho_j\,.$$

The equation of the locus for which $f(\tilde{\mathbf{g}})=0$ is therefore:

$$\sum_{j=1}^{1/2S_0}\cos 2\pi\mathbf{g}\,.\,\varrho_j=0\,. \tag{13a}$$

If the centre of symmetry is also a cluster site this relation becomes:

$$1+2\sum_{j=1}^{1/2S_0}\cos 2\pi\mathbf{g}\,.\,\varrho_j=0\,. \tag{13b}$$

If there is *no* centre of symmetry one has in general:

$$f(\mathbf{g})\equiv\varphi(\mathbf{g})+i\psi(\mathbf{g})$$

and the locus for which $f(\mathbf{g})=0$ is given by the curves along which the surfaces:

$$\varphi(\mathbf{g})=0 \text{ and } \psi(\mathbf{g})=0 \tag{14}$$

intersect. The explicit expressions for the equations of the geometrical loci of diffuse intensity corresponding to the different cluster types considered (Fig. 3) are tabulated in Table 2.

As a limiting case one can consider the whole crystal as a cluster, in which case the composition condition is necessarily satisfied. For a crystal with $N+1$ sites equation (11), disregarding effects due to its finite size, reduces to the well known relation:

$$\sum_{j=0}^{N}\alpha_j=0 \tag{16}$$

where the sum is taken over all lattice vectors. Condition (12) reduces to:

$$\sum_{j=0}^{N}\exp\left[2\pi i\mathbf{g}\,.\,\mathbf{r}_j\right]=0$$

Since $\sum_{j=0}^{N}\exp\left[2\pi i\mathbf{g}\,.\,\mathbf{r}_j\right]=\sum_k\delta(\mathbf{g}-\mathbf{g}_k)$ where $\mathbf{g}_k$ are the diffraction vectors of the Bragg reflexions, it is concluded that diffuse intensity due to SRO can be located everywhere in reciprocal space except at the Bragg reflexions.

4. Deviations from ideal composition

In reality it is to be expected that in the transition state not all clusters will have the ideal composition. This

Table 2. *Allowed location for diffuse intensity corresponding with different cluster types in the f.c.c. lattice*

	Cluster type	Cluster point positions ϱ_j	Geometric locus in reciprocal space $\mathbf{g}(h,k,l)$		Fig.
Centrosymmetrical	Octahedron	$\varrho_1=\pm\frac{1}{2}$ [100] $\varrho_2=\pm\frac{1}{2}$ [010] $\varrho_3=\pm\frac{1}{2}$ [001]	$\cos\pi h+\cos\pi k+\cos\pi l=0$	(15*a*)	3(*a*)
	Cube	$\varrho_1=\pm\frac{1}{2}$ [111] $\varrho_2=\pm\frac{1}{2}$ [11$\bar{1}$] $\varrho_3=\pm\frac{1}{2}$ [1$\bar{1}$1] $\varrho_4=\pm\frac{1}{2}$ [$\bar{1}$11]	$\cos\pi h\cos\pi k\cos\pi l=0$	(15*b*)	3(*b*)
	Planar 5-point cluster in cube plane	$\varrho_1=$[000] $\varrho_2=\pm\frac{1}{2}$ [110] $\varrho_3=\pm\frac{1}{2}$ [1$\bar{1}$0]	$1+4\cos\pi h\cos\pi k=0$	(15*c*)	3(*c*)
Non-centrosymmetrical	Tetrahedron of nearest neighbours	$\varrho_1=$[000] $\varrho_2=\frac{1}{2}$ [110] $\varrho_3=\frac{1}{2}$ [011] $\varrho_4=\frac{1}{2}$ [101]	$\cos\pi h/2\cos\pi k/2\cos\pi l/2=0$ $\sin\pi h/2\sin\pi k/2\sin\pi l/2=0$	(15*d*)	3(*d*)
	Pyramidal 5-point cluster	$\varrho_1=$[000] $\varrho_2=\frac{1}{2}$ [$\pm$101] $\varrho_3=\frac{1}{2}$ [0$\pm$11]	$\sin\pi l=0$ $\cos\pi h+\cos\pi k=-\frac{1}{2}$	(15*e*)	3(*e*)
	Irregular tetrahedron	$\varrho_1=$[000] $\varrho_2=$[001] $\varrho_3=\frac{1}{2}$ [101] $\varrho_4=\frac{1}{2}$ [011]	$2\cos\pi l+\cos\pi h+\cos\pi k=0$ $\sin\pi h+\sin\pi k=0$	(15*f*)	3(*f*)

can be due to the fact that the ideal composition is not realized in each cluster although it could be according to the overall composition of the alloy, or also that the overall composition is not compatible with the cluster size such that clusters with at least two different compositions must occur in a given proportion. We shall discuss in turn the effect of each circumstance.

(a) Non-ideal composition of the clusters

We shall assume that a fraction p_0 of the clusters have the ideal composition m_A and hence contain $S_0 m_A$ A atoms, whereas equal fractions p_1 and p_2 contain $m_A' S_0 = m_A S_0 - 1$ and $m_A'' S_0 = m_A S_0 + 1$ A atoms such that $m_A' + m_A'' = 2m_A$ and $p_0 + p_1 + p_2 = 1$ ($p_1 = p_2$).

Equation (4) now applies to each of the three kinds of clusters; one has:

$$\sum_{j=1}^{S_0} \bar{\sigma}_j' = -S_0(m_A' - m_A); \quad \sum_{j=1}^{S_0} \bar{\sigma}_j^0 = 0;$$

$$\sum_{j=1}^{S_0} \bar{\sigma}_j'' = -S_0(m_A'' - m_A)$$

and hence:

$$m_A m_B(S_0\alpha_0' + 2S_1\alpha_1' + 2S_2\alpha_2' + \ldots) = S_0^2(m_A' - m_A)^2$$
$$m_A m_B(S_0\alpha_0^0 + 2S_1\alpha_1^0 + 2S_2\alpha_2^0 + \ldots) = 0$$
$$m_A m_B(S_0\alpha_0'' + 2S_1\alpha_1'' + 2S_2\alpha_2'' + \ldots) = S_0^2(m_A'' - m_A)^2.$$

Noting that $\alpha_j = p_0\alpha_j^0 + p_1\alpha_j' + p_2\alpha_j''$ one obtains by combining the three last equations:

$$m_A m_B(S_0\alpha_0 + 2S_1\alpha_1 + 2S_2\alpha_2 + \ldots) = S_0^2[p_1(m_A' - m_A)^2 + p_2(m_A'' - m_A)^2]$$

or since $p_1 = p_2 = \frac{1}{2}(1 - p_0)$

$$S_0\alpha_0 + 2S_1\alpha_1 + 2S_2\alpha_2 + \ldots = (1 - p_0)/m_A m_B. \quad (17a)$$

The right-hand side which is zero in the ideal case, becomes larger as more clusters have a non-ideal composition.

(b) Composition non-compatible with cluster size

Let us now assume that the cluster size is non-compatible with the overall composition as is, for example,

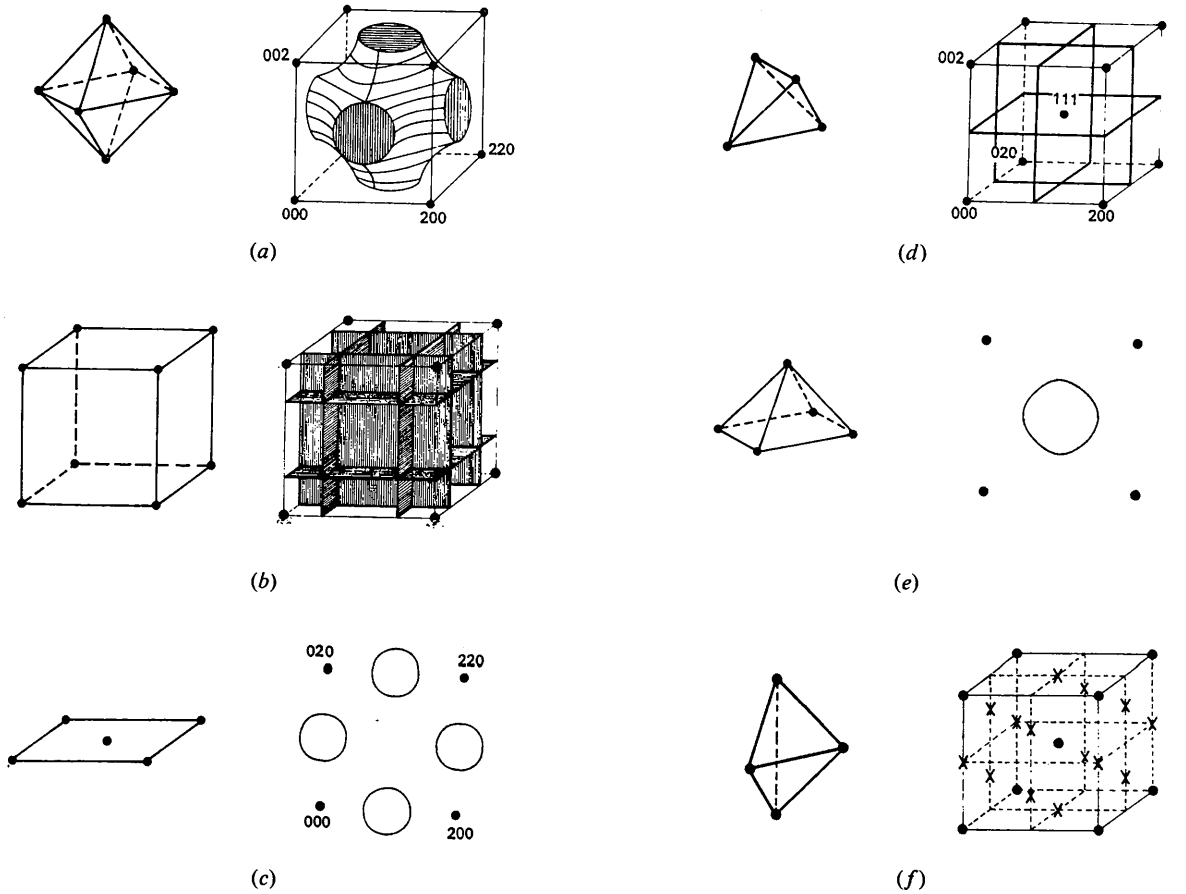

Fig. 3. Different cluster types (left) with their corresponding diffuse intensity distributions (right): (*a*) octahedron, (*b*) cube, (*c*) planar five-point cluster (only the intersection of the cylindrical surface with the [001] section is shown), (*d*) tetrahedron of nearest neighbours, (*e*) pyramidal five-point cluster, (*f*) irregular tetrahedron (only the intersection points with the cube planes are shown).

the case with octahedra in an A_3B alloy. In general it is sufficient to accept the occurrence of two kinds of clusters in the right fractions p' and p'' to achieve the macroscopic composition. One contains an integral number of A atoms $S_0 m_A' > S_0 m_A$ and the other an integral number of A atoms $S_0 m_A'' < S_0 m_A$ such that $m_A' S_0 + 1 = m_A'' S_0$ or $m_A'' - m_A' = (1/S_0)$. One has again for the two types of clusters separately:

$$\sum_{j=1}^{S_0} \bar{\sigma}_j = -S_0(m_A' - m_A); \quad \sum_{j=1}^{S_0} \bar{\sigma}_j = -S_0(m_A'' - m_A)$$

and hence:

$$m_A m_B[S_0\alpha_0' + 2S_1\alpha_1' + 2S_2\alpha_2'' + \ldots] = S_0^2(m_A - m_A')^2$$
$$m_A m_B[S_0\alpha_0'' + 2S_1\alpha_1'' + 2S_2\alpha_2'' + \ldots] = S_0^2(m_A - m_A'')^2 .$$

Since $\alpha_j = p'\alpha_j' + p''\alpha_j''$ with $p' + p'' = 1$ and $p' m_A' + p'' m_A'' = m_A$ one obtains by combining these equations:

$$S_0\alpha_0 + 2S_1\alpha_1 + 2S_2\alpha_2 + \ldots = [S_0^2/(m_A m_B)]\,[p'(m_A - m_A')^2 + p''(m_A'' - m_A)^2]$$

and since:

$$p' = (m_A'' - m_A)/(m_A'' - m_A') \text{ and } p'' = (m_A - m_A')/(m_A'' - m_A')$$

the right-hand side of the equation can be simplified and the relation reduces to:

$$S_0\alpha_0 + 2S_1\alpha_1 + 2S_2\alpha_2 + \ldots = (p'p'')/(m_A m_B). \quad (17b)$$

5. Effects of non-ideal cluster composition on the diffuse intensity distribution

Deviations from the ideal cluster composition cause the right-hand side of the equation (10) in both cases to differ from zero, *i.e.* the equation now becomes:

$$C\int_{V^*} I_D(\mathbf{g})F(\mathbf{g})\mathrm{d}\mathbf{g} = \delta$$

with either $\delta = (1 - p_0)/m_A m_B$ or $\delta = p'p''/m_A m_B$. In view of equation (9) one can always rewrite this as:

$$C\int_{V^*} I_D(\mathbf{g})[F(\mathbf{g}) - \delta]\mathrm{d}\mathbf{g} = 0 .$$

Whereas $F(\mathbf{g})$ is always non-negative, this is no longer the case for $F(\mathbf{g}) - \delta$ since $\delta \geq 0$. If δ is small compared to the average value of $F(\mathbf{g})$, the expression $F(\mathbf{g})$ will only be negative in a narrow region around $F(\mathbf{g}) = 0$. One can then still expect for continuity reasons that $I(\mathbf{g})$ will now be non-vanishing only in the vicinity of the surface $F(\mathbf{g}) - \delta = 0$. The effect of deviations from the ideal transition state described in our model is therefore to cause a deformation and/or a broadening of the distribution around the ideal one. It will be shown in a forthcoming paper that, if special ordering conditions are satisfied, the intensity is concentrated on the surface $F(\mathbf{g}) - \delta = 0$, even when the value of δ is large.

6. Application to alloy systems

It is quite natural to assume that the transition from the SRO state to the LRO state will occur gradually and that in a 'transition phase' clusters will be formed, which are a 'prefiguration' of the LRO state in that they are built from the same sub-unit-cell motifs and have predominantly the same composition as in the LRO state towards which they evolve. In §3 we have calculated analytical expressions for the loci of the diffuse intensity for different clusters of this type. It is to be expected that gradually more complicated clusters will become predominant and that finally, microdomains of LRO will form in a SRO matrix. This should be reflected in the evolution of the pattern of diffuse scattering due to these clusters. We shall now describe the evolution of this *transition state* for different alloys and propose interpretations for the observed patterns in terms of clusters and microdomains. (One should be careful when determining diffuse scattering configurations; several sections through reciprocal space are required to locate the spatial configuration with any precision.)

6.1 *The* Ni–Mo *system*

The Ni-rich end of the Ni–Mo system is of particular interest because the maxima in diffuse intensity due to SRO do not coincide with the positions of the LRO spots of the Ni_4Mo structure. Dark-field images in the SRO spots were first shown by Ruedl, Delavignette & Amelinckx (1968) to be spotty and attributed to the occurrence of microdomains of the different orientation variants. Later this was confirmed and discussed by a number of authors (Moss & Clapp, 1968; Okamoto & Thomas, 1971; Das & Thomas, 1974; Chakravarti, Starke, Sparks & Williams, 1974).

We have studied alloys of the two different compositions Ni_3Mo and Ni_4Mo. We first describe the evolution of the diffuse scattering patterns on isothermal annealing after quenching from above the ordering temperature. The alloys are water quenched as foils, annealed under vacuum at 800 °C or 840 °C for varying periods of time and subsequently thinned electrolytically before examination in the electron microscope. The results are somewhat different for the two compositions and for the two annealing temperatures. We therefore describe the phenomena in the two alloys separately and subsequently we propose an interpretation within the framework of our model.

(*a*) *The* Ni_4Mo *composition*

When quenched in direct contact with water, the foils exhibit a [001] pattern as shown in Fig. 5(*a*) *i.e.* with maxima at the $(1\frac{1}{2}0)$ positions only. Dark-field images in such spots do not reveal microdomains. When the alloy is water quenched in a quartz capsule, one obtains the pattern of Fig. 4(*a*) which is represented schematically in Fig. 5(*b*). Dark-field images in a $(1\frac{1}{2}0)$ spot now reveal microdomains. The pattern of

the type shown in Fig. 5(*a*) is therefore to be considered as a representation of the true SRO state, whereas the pattern of Fig. 5(*b*) is characteristic of a specimen containing a fine-scale microdomain structure.

The [001] pattern shown in Fig. 4(*a*) and schematically in Fig. 5(*b*) contains, apart from the SRO spots of type 1, pseudo-circles 2 and segments 3. These features are both situated in the cube planes as can be deduced from the oblique [112] sections of Fig. 4(*a*) which show diffuse streaks along the intersection of the planes *h*, *k* or *l*=integer. The [01$\bar{1}$] section of Fig. 6 is also consistent with this interpretation. It should be noted that in the [001] section the pseudo-circle does not pass through the spots 1, but lies slightly outside the square formed by spots of type 1. Since all the intensity is found to be in planes such as $l=0, \pm 1 \ldots$ the pseudo-circles are curves in reciprocal space; they are not due to the intersection of a surface in reciprocal space with Ewald's sphere.

On further annealing, either at 800°C or at 840°C the [001] and [112] patterns evolve as shown in Fig. 4(*b*) and schematically in Fig. 5(*c*) for the [001] pattern. The weak straight segments disappear first; afterwards the pseudo-circles increase slightly in size and then they break up into segments [Fig. 4(*c*)] connected to the type 1 spots. Finally the intensity becomes concentrated in the type 5 spots, with only weak type 1 spots subsisting [Fig. 4(*d*)]. After 5 min at 800°C the pattern becomes that of Fig. 4(*e*). This pattern is characteristic of the domain structure consisting of all variants of the LRO Ni_4Mo structure. The very weak spots 6 are due to double diffraction at overlapping antiparallel twins; this has been described by Ruedl *et al.*, (1968). The SRO spots 1 have now completely disappeared.

(*b*) Ni_3Mo *composition*

After quenching from above the ordering temperature the same SRO spots as in Ni_4Mo are present [Fig. 7(*a*)]. On annealing for about 5 min at 800°C the pattern of Fig. 7(*c*), which is schematically shown in Fig. 8(*c*), results. On annealing for the same period of time at 840°C, one obtains the pattern shown in Fig. 7(*b*) and represented schematically in Fig. 8(*b*).

Dark-field images taken in spots of the type 8 exhibit the 'precipitates' or 'domains' of Fig. 9(*a*), whereas dark-field images in spots of the type 5 reveal the 'microdomains' or 'precipitates' shown in Fig. 9(*b*). In the first case, the precipitates have the Ni_2Mo structure whereas in the second case the structure of the particles is that of Ni_4Mo. Of course only a fraction of the variants show up in each spot. The spots of type 8 are elongated along a direction which is tangential to the pseudo-circles of diffuse intensity.

(*c*) *Interpretation of the diffuse intensity patterns*

According to the conclusions of §3, a diffuse intensity distribution along segments defined by the relations $l=0$; $h,k=\pm 1$ (and similar ones derived from this one by symmetry) points to the presence of tetrahedral clusters (Table 2). The segments should be best defined in patterns from the alloy with a composition which is compatible with the composition of the clusters, *i.e.* in the Ni_3Mo alloy. In this alloy the cluster containing three Ni atoms and one Mo atom has the macroscopic composition. The diffuse segments are indeed found to be better defined in Ni_3Mo than in Ni_4Mo. In all cases the segments are very weak, however, and the tetrahedron does not seem to be a prominent feature except under special conditions leading to the formation of the DO_{22} structure, which has the composition 1–3 and which can be considered to be built from such regular tetrahedra as well as from irregular tetrahedra of the type considered in Table 2 (see Van Tendeloo, De Ridder & Amelinckx, 1975). The superlattice spots form along the diffuse segments at the intersection points of the two loci corresponding to regular and irregular tetrahedra.

The occurrence of the pseudo-circles 7 through the spots of the type 1 in Ni_3Mo can be attributed to the occurrence of regions of octahedral clusters. These regions cannot have the macroscopic composition; but they may for example have the compositions

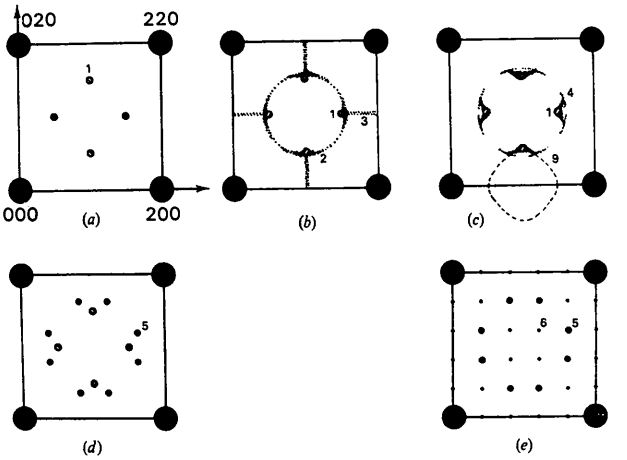

Fig. 5. Schematic representation of the [001] diffraction pattern for Ni_4Mo after different annealing times: (*a*) As-quenched in direct contact with water; only the SRO spots are present. (*b*) When specimens are quenched in quartz capsules supplementary diffuse intensity is observed [Fig. 4(*a*)]. (*c*), (*d*), (*e*) Schematic representation of the patterns of Figs. 4(*c*) (*d*), and (*f*) respectively.

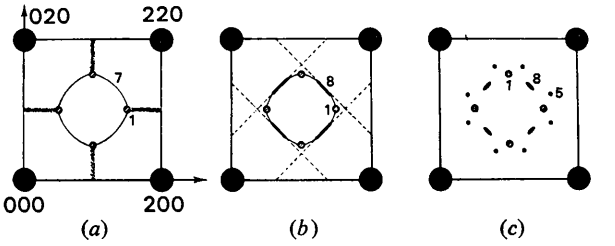

Fig. 8. Schematic representation of the [001] sections shown in Fig. 7.

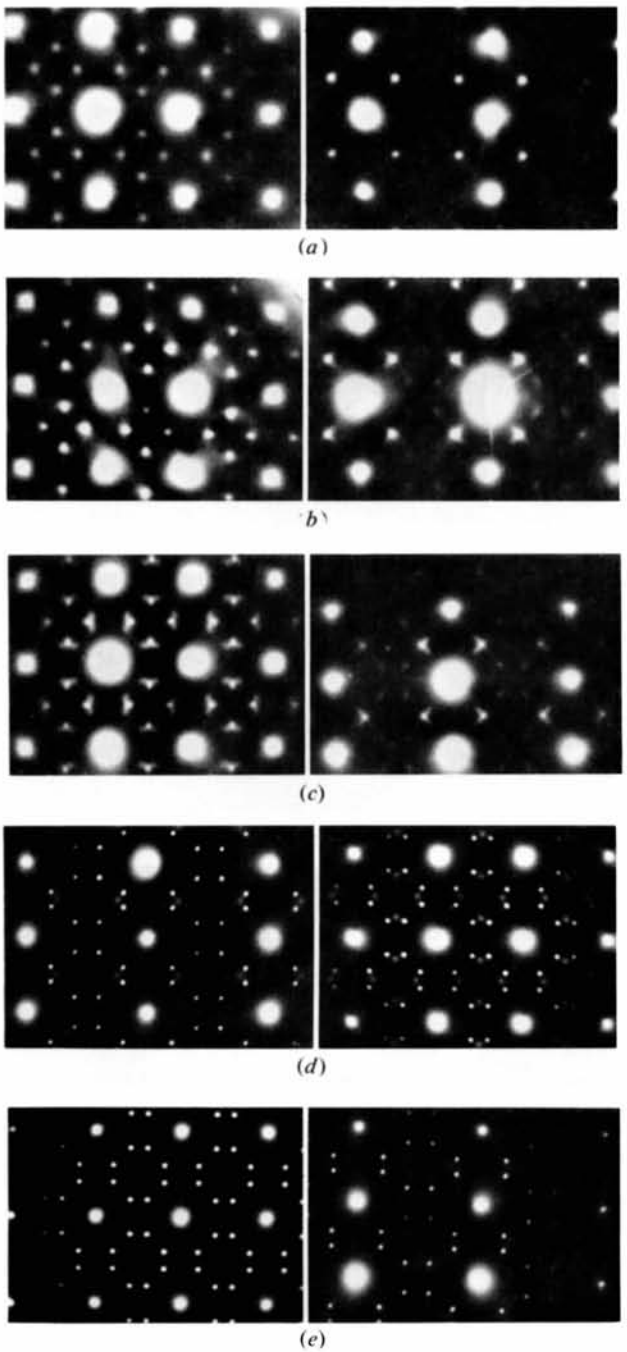

(*a*)

(*b*)

(*c*)

(*d*)

(*e*)

Fig. 4. [001] section (left) and [112] section (right) of the diffraction pattern for Ni_4Mo after different annealing times at 800 °C. (*a*) when quenched in a quartz capsule. (*b*), (*c*), (*d*), (*e*) after annealing 10, 30, 60 and 300 s respectively at 800 °C.

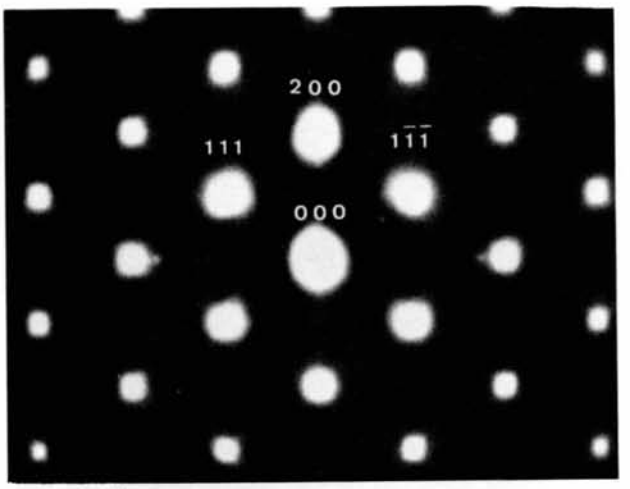

Fig. 6. [$01\bar{1}$] section of the Ni_4Mo diffraction pattern of an alloy quenched into water whilst being encapsulated in quartz. Note the horizontal diffuse streaks in the (022) direction.

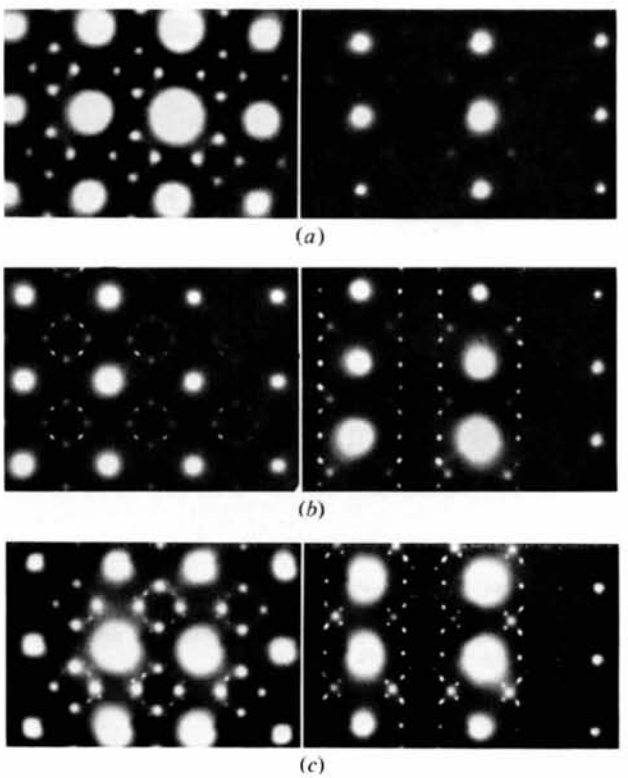

(*a*)

(*b*)

(*c*)

Fig. 7. [001] section (left) and [112] section (right) for Ni_3Mo (*a*) as quenched, (*b*) after annealing for 5 minutes at 840 °C, (*c*) after annealing for 5 minutes at 800 °C.

[*To face p.* 222

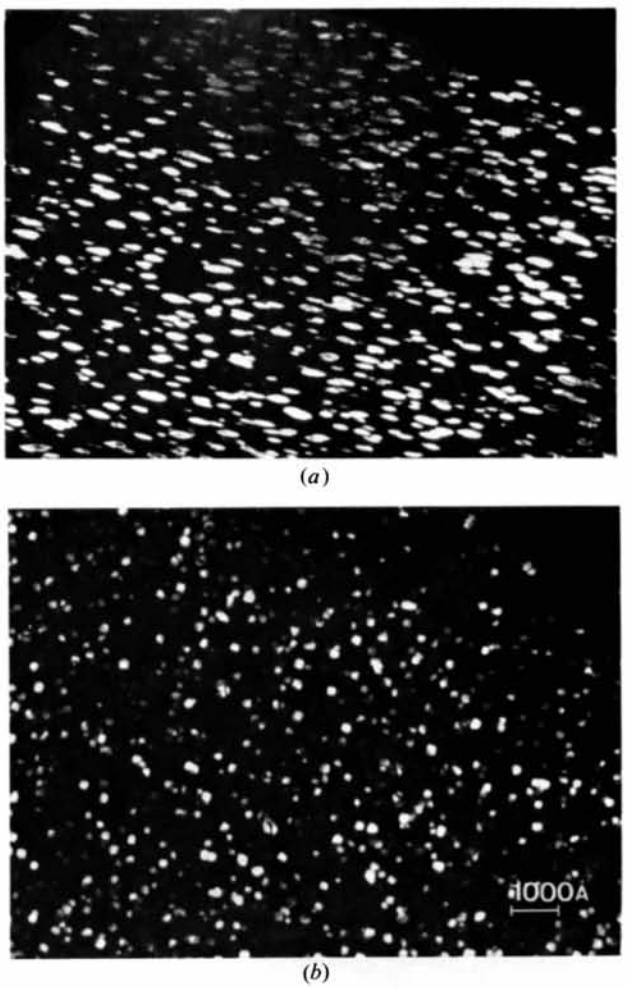

(a)

(b)

Fig. 9. Dark-field micrographs in a Ni_2Mo spot and a Ni_4Mo spot corresponding to the diffraction patterns of Figs. 7(*b*) and 7(*c*) respectively. Note the difference in morphology between the two domain structures.

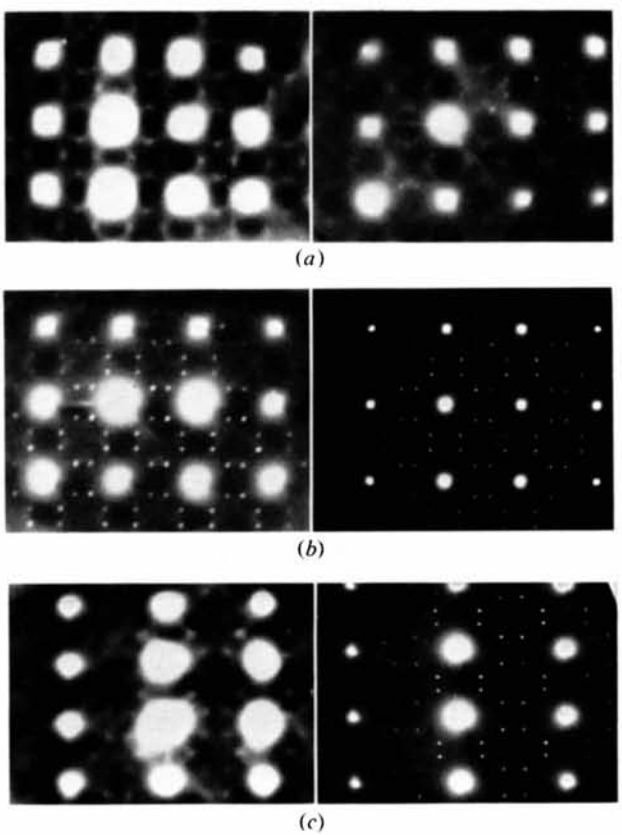

(a)

(b)

(c)

Fig. 12. (*a*) and (*b*) [001] section, (*c*) [112] section of the diffraction pattern for Au_4V at different stages between the as-quenched state and the completely ordered state.

Ni_4Mo_2 or Ni_5Mo. Since the diffuse intensity is concentrated in planes of the type [001] one-dimensional LRO along a cube direction is present, *i.e.* in these regions chains of Ni and Mo atoms are formed along one of the cube directions. As a result, diffuse intensity due to the transition state is located on pseudo-circles like:

$$\begin{cases} \cos \pi h + \cos \pi k + 1 = 0 \\ l = 0 . \end{cases}$$

Note that this curve passes through the four points 1.

In the Ni_3Mo alloy the appearance of the small streaks 8 [Fig. 7(*b*)] along the [110] direction can be interpreted as being due to the formation of a linear three-point cluster along one of the [110] directions. Such clusters are suggested by their occurrence in the Ni_2Mo structure, which can be built by means of linear three-point clusters with the macroscopic Ni_2Mo composition. Such clusters lead to diffuse intensity along planes of the type:

$$h + k = (\tfrac{2}{3}, \tfrac{4}{3}) + 2n (n = \text{integer})$$

which are tangents to the pseudo-circles. As a result the type 8 spots are streaked in the [110] directions in accord with observations of Yamamoto, Nenno, Sabury & Tizutani (1970). Previously this streaking was explained by Okamoto & Thomas (1971) as being the 'average' of two [210] type directions, perpendicular to the planes of non-conservative antiphase boundaries. The pseudo-circles 2 observed in Ni_4Mo patterns can be attributed to five-point clusters of the pyramidal type, describe in §3 and in the ideal case giving rise to diffuse intensity along the curves:

$$\begin{cases} \cos \pi h + \cos \pi k = -\frac{1}{2} \\ l = 0, \pm 1 \ldots \end{cases}$$

These clusters are suggested because they are present in the Ni_4Mo structure. If the macroscopic composition for such clusters is strictly imposed, one-dimensional LRO of the type occurring along the *c* direction in LRO Ni_4Mo, is automatically implied. This can be seen immediately on reference to Fig. 10. If the summit of the first Ni_4Mo pyramid 1 is occupied by Mo the base of the inverted pyramid 2 on top of this one is to be occupied exclusively by Ni, and as a result the top of the pyramid built on this base has again to be Mo. Automatically an infinite row of slightly tetragonal octahedra of the type occurring along the *c* axis in Ni_4Mo results. One therefore expects sequences of such pyramidal clusters, only interrupted by a cluster which has not the required composition. It is noteworthy that the computer simulation by Chakravarti *et al*, (1974) of SRO in Ni_4Mo also leads to similar rod-like microdomains along a cube direction. In order to generate the LRO state, ordering has to spread laterally, *i.e.* in planes perpendicular to the rows just considered. This will be initiated by the formation of a planar five-point cluster of the type described in Table 2. The occurrence of such clusters is therefore a natural assumption and has necessarily to arise somewhat later in the initial stage of ordering. The diffuse intensity associated with such clusters is concentrated along cylindrical surfaces represented in Fig. 3(*c*). The intersection of the pseudo-circle 2 with the cylindrical surface of type 9 indicated by the dotted line in Fig. 5(*c*), leads naturally to the formation of the wings 4 [Fig. 4(*c*)] and finally to the formation of the spots 5. This is consistent since the simultaneous presence of the pyramidal and planar five point clusters leads to domains of LRO structure. The five types of cluster considered as yet: (i) the tetrahedral cluster, (ii) the octahedral cluster, (iii) the linear [110] three-point cluster with composition Ni_2Mo, (iv) the pyramidal five-point cluster with composition Ni_4Mo, (v) the planar five-point cluster with composition Ni_4Mo apparently occur simultaneously in Ni_3Mo, whereas only (iv) and (v) occur predominantly in Ni_4Mo. We shall now describe the chronological appearance of these different clusters.

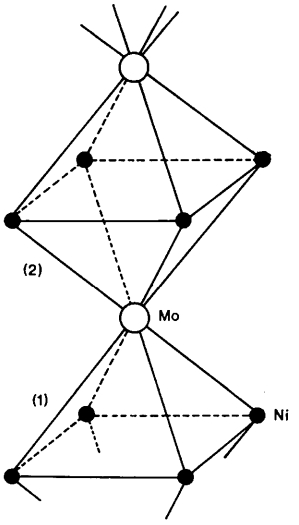

Fig. 10. Pyramidal cluster formation leading to LRO in the *c* direction. If the composition rule is not violated an infinite chain of octahedra results once the first pyramidal five-point cluster is formed.

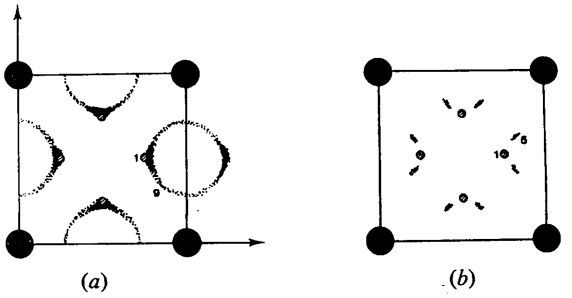

Fig. 11. Schematic representation of the [001] diffraction pattern for Au_4V (*a*) after quenching, (*b*) after annealing for 5 min.

For Ni_3Mo the linear clusters of type Ni_2Mo give rise to short segments of type 8, which are in fact due to the superposition of the lines associated with the linear three-point cluster and indicated by means of dotted lines in Fig. 5(*c*), and of the pseudo-circles 7 due to the octahedra. These segments 8 evolve into the spots due to the Ni_2Mo precipitates whereas the spots due to the different Ni_4Mo variants become visible as well in Fig. 7(*c*). As long as the SRO matrix subsists the four spots of type 1 remain as well.

In the Ni_4Mo alloy the evolution is simpler in that only one ordered phase is formed. The first clusters that form out of the SRO state are apparently the five-point pyramidal clusters that produce the pseudo-circle 2 (Figs. 4 and 5) and the tetrahedra that give rise to the segments 3. The latter clusters are apparently not stable because the segments 3 that reveal them rapidly disappear and the pseudo-circle breaks up into the short segments 4, which can be interpreted as being due to the intersection of the locus due to the pyramidal five-point cluster and that due to the planar five-point cluster (Fig. 3). Note that the spots due to the LRO Ni_4Mo structure are situated at the intersection points of the loci (15*e*) and (15*c*).

After longer annealing the microdomains grow and the spots 5 become sharper whereas the spots 1 finally disappear completely, corresponding to the elimination of the SRO matrix.

When making dark-field images in the segments of the pseudocircles 2 one observes a spotty pattern, suggesting that microdomains are characteristic of the 'transition' state, rather than of the true SRO state. The reason why microdomains have been observed initially in spots 1 by a number of authors, is presumably to be attributed to the fact that one inevitably also collects the most intense parts of the pseudo-circle 2 in the aperture when making dark-field images in type 1 spots.

6.2 *The Au–V system*

Although the gold–vanadium system at its Au-rich end gives rise to the same superstructure as Ni_4Mo, the behaviour of the 'transition' state is different from that in the Ni–Mo system.

In the as-quenched state, both Au_3V and Au_4V show the configuration of diffuse scattering represented schematically in Fig. 11 and reproduced in Fig. 12. The SRO spots are much more diffuse than in Ni_4Mo. The pseudo-circles 9 [Fig. 11(*a*)] do not pass through the SRO spots; but they do pass through the positions 5 which will be occupied in the LRO state by the eight superlattice spots. From the [112] section of reciprocal space [Fig. 12(*c*)] it can now be concluded that diffuse intensity is not located in planes as in the case of Ni_4Mo but along cylindrical surfaces parallel to the cube directions and which intersect the (001) plane along the pseudo-circles of Fig. 11(*a*). Such cylinders are of course present along all cube directions giving rise to loci in space which are the intersecting lines of these cylinders; along such lines, the diffuse intensity will be largest.

In Au_4V as well as in Au_3V, which behaves quite similarly, it thus seems that the planar five-point cluster is predominant in the initial stages of ordering. In a further stage the five-point pyramidal cluster forms and the superposition of the diffuse scattering patterns due to the two types of five-point cluster leads to the pattern of Fig. 11(*b*). The chronological order in which the five-point pyramidal and planar clusters appear is apparently inverted in Au_4V as compared to Ni_4Mo.

Conclusions

The diffuse scattering phenomena that accompany the 'transition' between the SRO state and the LRO state in alloys can be explained satisfactorily on the assumption that configurations of atoms are formed which prefigure the LRO structure. These configurations are predominantly clusters such as tetrahedra, octahedra, *etc*... formed by atoms placed on f.c.c. lattice positions, and satisfy the composition requirement. In general, these clusters which occur also in the LRO alloy constitute the predominant type and suffice to explain the observed diffuse scattering features.

References

BRUNEL, M., DE BERGEVIN, F. & GONTRAND, M. (1972). *J. Phys. Chem. Solids*, **33**, 1927–1941.

CHAKRAVARTI, B., STARKE, E. A. JR, SPARKS, C. J. JR & WILLIAMS, R. O. (1974). *J. Phys. Chem. Solids*, **35**, 1317–1326.

CLAPP, P. C. (1971). *Phys. Rev.* B4, **2**, 255–270.

CLAPP, P. C. & MOSS, S. C. (1966). *Phys. Rev.* **142**, 418–427.

COWLEY, J. M. (1950). *J. Appl. Phys.* **21**, 24–30.

DAS, S. K. & THOMAS, G. (1974). *Phys. Stat. Sol.* (*a*), **21**, 177–190.

FLINN, P. A. (1956). *Phys. Rev.* **104**, 350–356.

GEHLEN, P. C. & COHEN, J. B. (1965). *Phys. Rev.* **139**, 844–855.

GRAGG, J. E., BARDHAN, P. & COHEN, J. B. (1971). *Critical Phenomena in Alloys, Magnets and Superconductors.* Edited by R. E. MILLS, E. ASCHER & R. I. JAFFEE. p. 309. New York: McGraw-Hill.

MOSS, S. C. (1964). *J. Appl. Phys.* **35**, 3547–3553.

MOSS, S. C. & CLAPP, A. C. (1968). *Phys. Rev.* **171**, 764–777.

OKAMOTO, P. R. & THOMAS, G. (1971). *Acta Met.* **19**, 825–841.

PAULING, L. (1960). *The Nature of the Chemical Bond*, 3rd ed. p. 547. Ithaca: Cornell Univ. Press.

RUEDL, E., DELAVIGNETTE, P. & AMELINCKX, S. (1968). *Phys. Stat. Sol.* **28**, 305–328.

SAUVAGE, M. & PARTHÉ, E. (1974). *Acta Cryst.* A**30**, 239–246.

VAN TENDELOO, G., DE RIDDER, R. & AMELINCKX, S. (1975). *Phys. Stat. Sol.* (*a*), **27**, 457–468.

WARREN, B. E. (1969). *X-ray Diffraction*, p. 277. Reading, Mass.: Addison Wesley.

YAMAMOTO, M., NENNO, S., SABURY, R. & TIZUTANI, Y. (1970). *Trans. Jap. Inst. Metals*, **11**, 120–126.